Numerically exact, time-dependent study of correlated electron transport in model molecular junctions

Haobin Wang and Michael Thoss

Citation: J. Chem. Phys. **138**, 134704 (2013); doi: 10.1063/1.4798404
View online: http://dx.doi.org/10.1063/1.4798404
View Table of Contents: http://jcp.aip.org/resource/1/JCPSA6/v138/i13
Published by the American Institute of Physics.

Numerically exact, time-dependent study of correlated electron transport in model molecular junctions

Haobin Wang[1] and Michael Thoss[2]
[1]*Beijing Computational Science Research Center, No. 3 He-Qing Road, Hai-Dian District, Beijing 100084, People's Republic of China and Department of Chemistry and Biochemistry, MSC 3C, New Mexico State University, Las Cruces, New Mexico 88003, USA*
[2]*Institute for Theoretical Physics and Interdisciplinary Center for Molecular Materials, Friedrich-Alexander-Universität Erlangen-Nürnberg, Staudtstr. 7/B2, D-91058 Erlangen, Germany*

(Received 17 January 2013; accepted 13 March 2013; published online 2 April 2013)

The multilayer multiconfiguration time-dependent Hartree theory within second quantization representation of the Fock space is applied to study correlated electron transport in models of single-molecule junctions. Extending previous work, we consider models which include both electron-electron and electronic-vibrational interaction. The results show the influence of the interactions on the transient and the stationary electrical current. The underlying physical mechanisms are analyzed in conjunction with the nonequilibrium electronic population of the molecular bridge. © *2013 American Institute of Physics*. [http://dx.doi.org/10.1063/1.4798404]

I. INTRODUCTION

The process of charge transport in molecular junctions has received much attention recently.[1–10] Single molecule junctions, consisting of single molecules that are chemically bound to metal electrodes, are well-suited systems to study nonequilibrium transport phenomena at the nanoscale and are also of interest for potential applications in the field of molecular electronics. Recent developments in experimental techniques, such as electromigration, mechanically controllable break junctions, or scanning tunneling microscopy,[1,11–28] have made it possible to study transport properties of molecular junctions. The rich experimental observations, e.g., Coulomb blockade,[13] Kondo effect,[29] negative differential resistance,[26,30,31] switching and hysteresis,[32–34] have stimulated many theoretical developments for understanding quantum transport at the molecular scale.

A particular challenge for the theory of charge transport in molecular junctions is the accurate treatment of correlation effects beyond the mean-field level. In molecular junctions, there are two types of correlation effects due to electronic-vibrational and electron-electron interaction. Considering vibrational induced correlation effects, a variety of theoretical approaches have been developed, including scattering theory,[35–42] nonequilibrium Green's function (NEGF) approaches,[43–51] and master equation methods.[43,52–64] In spite of the physical insight offered by these methods, all of them involve significant approximations. For example, NEGF methods and master equation approaches are usually based on (self-consistent) perturbation theory and/or employ factorization schemes. Scattering theory approaches to vibrationally coupled electron transport, on the other hand, neglect vibrational nonequilibrium effects and are limited to the treatment of a small number of vibrational degrees of freedom. These shortcomings have motivated us to develop a systematic, numerically exact methodology to study quantum dynamics and quantum transport including many-body effects—the multilayer multiconfiguration time-dependent Hartree (ML-MCTDH) theory in second quantization representation (SQR).[65] For a generic model of vibrationally coupled electron transport, we have demonstrated the importance of treating electronic-vibrational coupling accurately. Comparison with approximate methods such as NEGF reveals the necessity of employing accurate methods such as the ML-MCTDH-SQR theory, in particular in the strong coupling regime.

In this paper, we extend the ML-MCTDH-SQR method to treat the electron-electron interaction. Considering the paradigmatic Anderson impurity model, we show the applicability of the methodology to obtain an accurate description. Furthermore, we consider a model which incorporates both electron-electron and electronic-vibrational interaction. To the best of our knowledge, the nonequilibrium results reported for this model are the first obtained by a numerically exact method.

It is noted that a variety of other powerful methods have been developed in the recent years with the same goal, i.e., to facilitate numerically exact simulations for nonequilibrium transport in model systems. These include the numerical path integral approach,[66–68] real-time quantum Monte Carlo simulations,[69,70] the numerical renormalization group approach,[71] the time-dependent density matrix renormalization group approach,[72] the hierarchical equations of motion method,[73,74] and a combination of reduced density matrix techniques and impurity solvers.[75] For a comparison and a comprehensive overview of various different methods in the case of nonequilibrium transport with electron-electron interaction see Ref. 76.

The remaining part of the paper is organized as follows. Section II outlines the physical model and the observables of interest. The ML-MCTDH-SQR theory is described in Sec. III. Section IV presents numerical results for a variety of parameter regimes as well as an analysis of the transport mechanisms. Finally, Sec. V concludes with a summary.

II. MODEL AND OBSERVABLES OF INTEREST

To study correlated electron transport in molecular junctions, we consider a generic model which includes both electron-electron and electronic-vibrational interaction. The model comprises two discrete electronic states (spin up and down) at the molecular bridge, two electronic continua describing the left and the right metal leads, respectively, and a distribution of harmonic oscillators that models the vibrational modes of the molecular bridge. The Hamiltonian reads

$$\hat{H} = \hat{H}_{\rm el} + \hat{H}_{\rm nuc} + \hat{H}_{\rm el-nuc}, \tag{2.1a}$$

where $\hat{H}_{\rm el}$, $\hat{H}_{\rm nuc}$, and $\hat{H}_{\rm el-nuc}$ describe the electronic degrees of freedom, the nuclear vibrations, and their coupling terms, respectively,

$$\begin{aligned}\hat{H}_{\rm el} = &\sum_{\sigma} E_d \hat{n}_{d,\sigma} + U_d \hat{n}_{d,\uparrow}\hat{n}_{d,\downarrow} + \sum_{k_L,\sigma} E_{k_L}\hat{n}_{k_L,\sigma} \\ &+ \sum_{k_R,\sigma} E_{k_R}\hat{n}_{k_R,\sigma} \\ &+ \sum_{k_L,\sigma} V_{dk_L}\left(\hat{d}_\sigma^+ \hat{c}_{k_L,\sigma} + \hat{c}_{k_L,\sigma}^+ \hat{d}_\sigma\right) \\ &+ \sum_{k_R,\sigma} V_{dk_R}\left(\hat{d}_\sigma^+ \hat{c}_{k_R,\sigma} + \hat{c}_{k_R,\sigma}^+ \hat{d}_\sigma\right),\end{aligned} \tag{2.1b}$$

$$\hat{H}_{\rm nuc} = \frac{1}{2}\sum_j \left(\hat{P}_j^2 + \omega_j^2 \hat{Q}_j^2\right), \tag{2.1c}$$

$$\hat{H}_{\rm el-nuc} = \sum_{\sigma} \hat{n}_{d,\sigma} \sum_j 2c_j \hat{Q}_j. \tag{2.1d}$$

In the above expression $\hat{n}$ denotes the number operator, subscript "d" refers to the bridge state, "k_L/k_R" the states of the left/right metal leads, and "$\sigma = \uparrow, \downarrow$" the two spin states. Operators $\hat{d}^+/\hat{d}$, $\hat{c}_{k_L}^+/\hat{c}_{k_L}$, $\hat{c}_{k_R}^+/\hat{c}_{k_R}$ are the fermionic creation/annihilation operators for the electronic states on the molecular bridge, the left and the right leads, respectively. The second term in (2.1b) describes the on-site Coulomb repulsion of the electrons on the molecular bridge with electron-electron coupling strength U_d. The energies of the electronic states in the leads, E_{k_L}, E_{k_R}, as well as the molecule-lead coupling parameters V_{dk_L}, V_{dk_R} are assumed to be independent of the spin polarization and are defined through the energy-dependent level width functions

$$\begin{aligned}\Gamma_L(E) &= 2\pi \sum_{k_L} |V_{dk_L}|^2 \delta(E - E_{k_L}), \\ \Gamma_R(E) &= 2\pi \sum_{k_R} |V_{dk_R}|^2 \delta(E - E_{k_R}).\end{aligned} \tag{2.2}$$

Without electronic-vibrational interaction the model introduced above reduces to the well-known Anderson impurity model,[77] which has been investigated in great detail both in equilibrium and nonequilibrium.[76,78] Neglecting, on the other hand, electron-electron interaction, it corresponds to the standard model of vibrationally coupled electron transport in molecular junctions, which has also been studied in great detail, mostly based on approximate methods. Recently a numerically exact treatment of the latter model (i.e., without electron-electron interaction) became possible using path integral techniques,[66,79] as well as the ML-MCTDH approach.[65,79,80] To the best of our knowledge, nonequilibrium transport of the full model, including both the electron-electron and electronic-vibrational interaction, has so far not been considered with numerically exact methods.

In principle, the parameters of the model can be obtained for a specific molecular junction employing first-principles electronic structure calculations.[81] In this paper, which focuses on the methodology and general transport properties, however, we will use a generic parameterization. Employing a tight-binding model, the function $\Gamma(E)$ is given as

$$\Gamma(E) = \begin{cases} \frac{\alpha_e^2}{\beta_e^2}\sqrt{4\beta_e^2 - E^2} & |E| \le 2|\beta_e| \\ 0 & |E| > 2|\beta_e| \end{cases}, \tag{2.3a}$$

$$\Gamma_L(E) = \Gamma(E - \mu_L), \quad \Gamma_R(E) = \Gamma(E - \mu_R), \tag{2.3b}$$

where β_e and α_e are nearest-neighbor couplings between two lead sites and between the lead and the bridge state, respectively. The width functions for the left and the right leads are obtained by shifting $\Gamma(E)$ relative to the chemical potentials of the corresponding leads. We consider a simple model of two identical leads, in which the chemical potentials are given by

$$\mu_{L/R} = E_f \pm V/2, \tag{2.4}$$

where V is the source-drain bias voltage and E_f is the Fermi energy of the leads. Since only the difference $E_d - E_f$ is physically relevant, we set $E_f = 0$.

Similarly, the frequencies ω_j and electronic-nuclear coupling constants c_j of the vibrational modes of the molecular junctions are modeled by a spectral density function[82,83]

$$J(\omega) = \frac{\pi}{2}\sum_j \frac{c_j^2}{\omega_j}\delta(\omega - \omega_j). \tag{2.5}$$

In this paper, the spectral density is chosen in Ohmic form with an exponential cutoff

$$J_{\rm O}(\omega) = \frac{\pi}{2}\alpha\omega e^{-\omega/\omega_c}, \tag{2.6}$$

where α is the dimensionless Kondo parameter.

Both the electronic and the vibrational continua can be discretized by choosing a density of states $\rho_e(E)$ and a density of frequencies $\rho(\omega)$ such that[84–86]

$$\int_0^{E_k} dE\ \rho_e(E) = k, \quad |V_{dk}|^2 = \frac{\Gamma(E_k)}{2\pi\rho_e(E_k)}, \quad k = 1, \ldots, N_e, \tag{2.7a}$$

$$\int_0^{\omega_j} d\omega\ \rho(\omega) = j, \quad \frac{c_j^2}{\omega_j} = \frac{2}{\pi}\frac{J_{\rm O}(\omega_j)}{\rho(\omega_j)}, \quad j = 1, \ldots, N_b, \tag{2.7b}$$

where N_e is the number of electronic states (for a single spin/single lead) and N_b is the number of bath modes in the

simulation. In this work, we choose a constant $\rho_e(E)$, i.e., an equidistant discretization of the interval $[-2\beta_e, 2\beta_e]$, to discretize the electronic continuum. For the vibrational bath, $\rho(\omega)$ is chosen as

$$\rho(\omega) = \frac{N_b + 1}{\omega_c} e^{-\omega/\omega_c}. \tag{2.8}$$

Within a given time scale the numbers of electronic states and bath modes are systematically increased to reach converged results for the quantum dynamics in the extended condensed phase system. In our calculations we employ 80-500 states for each electronic lead, implying 40-250 electrons per lead, and a bath with 100-400 modes.

The observable of interest for studying transport through molecular junctions is the current for a given source-drain bias voltage, given by (in this paper we use atomic units where $\hbar = e = 1$)

$$I_L(t) = -\frac{dN_L(t)}{dt} = -\frac{1}{\mathrm{tr}[\hat{\rho}]}\mathrm{tr}\{\hat{\rho} e^{i\hat{H}t} i[\hat{H}, \hat{N}_L] e^{-i\hat{H}t}\}, \tag{2.9a}$$

$$I_R(t) = \frac{dN_R(t)}{dt} = \frac{1}{\mathrm{tr}[\hat{\rho}]}\mathrm{tr}\{\hat{\rho} e^{i\hat{H}t} i[\hat{H}, \hat{N}_R] e^{-i\hat{H}t}\}. \tag{2.9b}$$

Here, $N_{L/R}(t)$ denotes the time-dependent charge in each lead, defined as

$$N_\zeta(t) = \frac{1}{\mathrm{tr}[\hat{\rho}]}\mathrm{tr}[\hat{\rho} e^{i\hat{H}t} \hat{N}_\zeta e^{-i\hat{H}t}], \quad \zeta = L, R, \tag{2.10}$$

and $\hat{N}_\zeta = \sum_{k_\zeta,\sigma} \hat{n}_{k_\zeta,\sigma}$ is the occupation number operator for the electrons in each lead ($\zeta = L, R$). For Hamiltonian (2.1) the explicit expression for the current operator is given as

$$\hat{I}_\zeta \equiv i[\hat{H}, \hat{N}_\zeta] = i \sum_{k_\zeta,\sigma} V_{dk_\zeta}\left(\hat{d}^+_\sigma \hat{c}_{k_\zeta,\sigma} - \hat{c}^+_{k_\zeta,\sigma}\hat{d}_\sigma\right), \quad \zeta = L, R. \tag{2.11}$$

In the expressions above, $\hat{\rho}$ denotes the initial density matrix representing a grand-canonical ensemble for each lead and a certain preparation for the bridge state

$$\hat{\rho} = \hat{\rho}^0_d \exp[-\beta(\hat{H}_0 - \mu_L \hat{N}_L - \mu_R \hat{N}_R)], \tag{2.12a}$$

$$\hat{H}_0 = \sum_{k_L,\sigma} E_{k_L} \hat{n}_{k_L,\sigma} + \sum_{k_R,\sigma} E_{k_R} \hat{n}_{k_R,\sigma} + \hat{H}^0_{\mathrm{nuc}}. \tag{2.12b}$$

Here $\hat{\rho}^0_d$ is the initial reduced density matrix for the bridge state, which is usually chosen as a pure state representing an occupied or an empty bridge state, and $\hat{H}^0_{\mathrm{nuc}}$ defines the initial bath equilibrium distribution.

Various initial states can be considered. For example, one may choose an initially unoccupied bridge state and the nuclear degrees of freedom equilibrated with this state, i.e. an unshifted bath of oscillators with $\hat{H}^0_{\mathrm{nuc}}$ as given in Eq. (2.1c). On the other hand, one may also start with a fully occupied bridge state and a bath of oscillators in equilibrium with the occupied bridge state

$$\hat{H}^{0'}_{\mathrm{nuc}} = \frac{1}{2}\sum_j \left[P_j^2 + \omega_j^2 \left(Q_j + 2\frac{c_j}{\omega_j^2} \right)^2 \right]. \tag{2.13}$$

Other initial states may also be prepared. The initial state may affect the transient dynamics profoundly. The dependence of the steady-state current on the initial density matrix is a more complex issue. Recent investigations for a model without electron-electron interaction seem to indicate that different initial states may lead to different (quasi)steady states,[79,87,88] although this has been debated.[89] Even without coupling to a vibrational bath, the initial bridge state population may still affect the final stationary current in a time-dependent simulation.[90,91] For all results reported in this paper, our calculations show that the stationary state is independent on the initial condition within the error bar of the simulation (which is estimated to be less than 10% relative error). Since different sets of initial conditions also affect the time scale at which the current $I(t)$ reaches its stationary value, we typically choose initial conditions that are close to the final steady state, e.g., an unoccupied initial bridge state if its energy is higher than the Fermi level of the leads and an occupied bridge state otherwise.

The transient behavior of the thus defined currents $I_R(t)$ and $I_L(t)$ is usually different. However, the long-time limits of $I_R(t)$ and $I_L(t)$, which define the stationary current, are the same. It is found that the average current

$$I(t) = \frac{1}{2}[I_R(t) + I_L(t)], \tag{2.14}$$

provides better numerical convergence properties by minimizing the transient characteristic, and thus will be used in most calculations.

In our simulations the continuous set of electronic states of the leads is represented by a finite number of states. The number of states required to properly describe the continuum limit depends on the time t. The situation is thus similar to that of a quantum reactive scattering calculation in the presence of a scattering continuum, where, with a finite number of basis functions, an appropriate absorbing boundary condition is added to mimic the correct outgoing Green's function.[92–95] Employing the same strategy for the present problem, the regularized electric current is given by

$$I^{\mathrm{reg}} = \lim_{\eta\to 0^+} \int_0^\infty dt\, \frac{dI(t)}{dt} e^{-\eta t}. \tag{2.15}$$

The regularization parameter η is similar (though not identical) to the formal convergence parameter in the definition of the Green's function in terms of the time evolution operator

$$G(E^+) = \lim_{\eta\to 0^+} (-i) \int_0^\infty dt\, e^{i(E+i\eta-H)t}. \tag{2.16}$$

In numerical calculations, η is chosen in a similar way as the absorbing potential used in quantum scattering calculations.[92–95] In particular, the parameter η has to be large enough to accelerate the convergence but still sufficiently small in order not to affect the correct result. While in the reactive scattering calculation η is often chosen to be coordinate dependent, in our simulation η is chosen to be time dependent

$$\eta(t) = \begin{cases} 0 & (t < \tau) \\ \eta_0 \cdot (t - \tau)/t & (t > \tau). \end{cases} \tag{2.17}$$

Here η_0 is a damping constant and τ is a cutoff time beyond which a steady state charge flow is approximately reached. As the number of electronic states increases, one may choose a weaker damping strength η_0 and/or longer cutoff time τ. The former approaches zero and the latter approaches infinity for an infinite number of states. In practice, for the systems considered in this work, convergence can be reached with a reasonable number of electronic states in the range of 80-500, with a typical τ = 30-80 fs (a smaller τ for less number of states) and $1/\eta_0$ = 3-10 fs.

To gain insight into the transport mechanisms, it is also useful to consider the population of the electronic states localized on the molecular bridge, which is given by

$$P_d(t) = \frac{1}{\mathrm{tr}[\hat{\rho}]}\mathrm{tr}\left\{\hat{\rho}e^{i\hat{H}t}\sum_{\sigma}\hat{n}_{d,\sigma}\,e^{-i\hat{H}t}\right\}. \tag{2.18}$$

III. THE MULTILAYER MULTICONFIGURATION TIME-DEPENDENT HARTREE THEORY IN SECOND QUANTIZATION REPRESENTATION

The time-dependent study of transport properties in the model introduced above requires a method that is able to describe many-body quantum dynamics in an accurate and efficient way. For this purpose we employ the recently proposed ML-MCTDH-SQR,[65,80] which allows a numerically exact treatment of the many-body problem. The method is based on the ML-MCTDH theory,[84] which is a rigorous variational method to propagate wave packets in complex systems with many degrees of freedom. In the variational calculation the wave function is represented by a recursive, layered expansion,

$$|\Psi(t)\rangle = \sum_{j_1}\sum_{j_2}\cdots\sum_{j_p} A_{j_1 j_2 \ldots j_p}(t)\prod_{\kappa=1}^{p}\left|\varphi_{j_\kappa}^{(\kappa)}(t)\right\rangle, \tag{3.1a}$$

$$\left|\varphi_{j_\kappa}^{(\kappa)}(t)\right\rangle = \sum_{i_1}\sum_{i_2}\cdots\sum_{i_{Q(\kappa)}} B^{\kappa,j_\kappa}_{i_1 i_2 \ldots i_{Q(\kappa)}}(t)\prod_{q=1}^{Q(\kappa)}\left|v_{i_q}^{(\kappa,q)}(t)\right\rangle, \tag{3.1b}$$

$$\left|v_{i_q}^{(\kappa,q)}(t)\right\rangle = \sum_{\alpha_1}\sum_{\alpha_2}\cdots\sum_{\alpha_{M(\kappa,q)}} C^{\kappa,q,i_q}_{\alpha_1\alpha_2\ldots\alpha_{M(\kappa,q)}}(t)\prod_{\gamma=1}^{M(\kappa,q)}\left|\xi_{\alpha_\gamma}^{\kappa,q,\gamma}(t)\right\rangle, \tag{3.1c}$$

$$\ldots$$

where $A_{j_1 j_2 \ldots j_p}(t)$, $B^{\kappa,j_\kappa}_{i_1 i_2 \ldots i_{Q(\kappa)}}(t)$, $C^{\kappa,q,i_q}_{\alpha_1\alpha_2\ldots\alpha_{M(\kappa,q)}}(t)$ and so on are the expansion coefficients for the first, second, third, …, layers, respectively; $|\varphi_{j_\kappa}^{(\kappa)}(t)\rangle$, $|v_{i_q}^{(\kappa,q)}(t)\rangle$, $|\xi_{\alpha_\gamma}^{\kappa,q,\gamma}(t)\rangle$, …, are the "single particle" functions (SPFs) for the first, second, third, … layers. In Eq. (3.1a), p denotes the number of single particle (SP) groups/subspaces for the first layer. Similarly, $Q(\kappa)$ in Eq. (3.1b) is the number of SP groups for the second layer that belongs to the κth SP group in the first layer, i.e., there are a total of $\sum_{\kappa=1}^{p} Q(\kappa)$ second layer SP groups. Continuing along the multilayer hierarchy, $M(\kappa, q)$ in Eq. (3.1c) is the number of SP groups for the third layer that belongs to the qth SP group of the second layer and the κth SP group of the first layer, resulting in a total of $\sum_{\kappa=1}^{p}\sum_{q=1}^{Q(\kappa)} M(\kappa, q)$ third layer SP groups. Naturally, the size of the system that the ML-MCTDH theory can treat increases with the number of layers in the expansion. In principle, such a recursive expansion can be carried out to an arbitrary number of layers. The multilayer hierarchy is terminated at a particular level by expanding the SPFs in the deepest layer in terms of time-independent configurations, each of which may contain several degrees of freedom.

The variational parameters within the ML-MCTDH theoretical framework are dynamically optimized through the use of the Dirac-Frenkel variational principle[96]

$$\langle\delta\Psi(t)|i\frac{\partial}{\partial t} - \hat{H}|\Psi(t)\rangle = 0,$$

which results in a set of coupled, nonlinear differential equations for the expansion coefficients for all layers.[65,80,84] For an N-layer version of the ML-MCTDH theory there are $N + 1$ levels of expansion coefficients. The introduction of this recursive, dynamically optimized layering scheme in the ML-MCTDH wavefunction provides more flexibility in the variational functional, which results in a tremendous gain in our ability to study large many-body quantum systems. During the past few years, significant progress has been made in further development of the theory to simulate quantum dynamics and nonlinear spectroscopy of ultrafast electron transfer reactions in condensed phases.[97–108] The theory has also been generalized to study heat transport in molecular junctions[109] and to calculate rate constants for model proton transfer reactions in molecules in solution.[110,111] Recent work of Manthe has introduced an even more adaptive formulation based on a layered correlation discrete variable representation (CDVR).[112,113]

The ML-MCTDH-SQR theory extends the original ML-MCTDH approach to systems of identical quantum particles by incorporating the exchange symmetry explicitly. This is different from the wave function-based approaches such as the MCTDHF approach[114–116] for treating identical fermions or the MCTDHB approach[117] for treating identical bosons that are incompatible with the multilayer idea in the ML-MCTDH theory.[65,84,97] Instead, a fundamentally different route is adopted in the ML-MCTDH-SQR theory[65]—an operator-based method that employs the second quantization formalism of many-particle quantum theory. This differs from many previous methods where the second quantization formalism is only used as a convenient tool to derive intermediate expressions for the first quantized form. In the new approach the variation is carried out entirely in the abstract Fock space using the occupation number representation. Therefore, the burden of handling symmetries of identical particles in a numerical variational calculation is shifted completely from wave functions to the algebraic properties of operators.

The major difference between the ML-MCTDH-SQR theory for identical fermions and the previous ML-MCTDH theory for distinguishable particles is the way how operators act. In practical implementation the symmetry of identical particles is realized by enforcing the algebraic anti-commutation relations of the fermionic creation/annihilation

operators

$$\{\hat{a}_P, \hat{a}_Q^+\} \equiv \hat{a}_P \hat{a}_Q^+ + \hat{a}_Q^+ \hat{a}_P = \delta_{PQ}, \quad \{\hat{a}_P^+, \hat{a}_Q^+\} = \{\hat{a}_P, \hat{a}_Q\} = 0. \tag{3.2}$$

This can be accomplished by introducing a permutation sign operator[65] associated with each fermionic creation/annihilation operator, which incorporates the sign changes of the remaining spin orbitals in all the SPFs whose subspaces are prior to it. The implementation is sophisticated but nonetheless can be reduced to handling (many and complicated) basic building blocks in the ML-MCTDH theory—products of operators. Thereby, the action of each Hamiltonian term (product of creation/annihilation operators) can be split into a series of operations on individual Fock subspaces.[65] On the other hand, for identical bosons the implementation is much simpler because there is no sign change upon permutation. A very important feature of the ML-MCTDH-SQR theory is that the equations of motion retain the same form as in the original ML-MCTDH theory.

Although formally the second quantized picture does not introduce new physics comparing with the first quantized framework, the efficiency of solving a problem is different. In the second quantized form, the wave function is represented in the abstract Fock space employing the occupation number basis. As a result, it can be expanded in the same multilayer form as that for systems of distinguishable particles. It is thus possible to extend the numerically exact treatment to much larger systems. The symmetry of the wave function in the first quantized form is shifted to the operator algebra in the second quantized form. The key point is that, for both phenomenological models and more fundamental theories, there are only a limited number of combination of fundamental operators. For example, in electronic structure theory only one- and two-electron operators are present. This means that one never needs to handle all, redundant possibilities of operator combinations as offered by the determinant form in the first quantized framework. It is exactly this property that provides the flexibility of representing the wave functions in multilayer form and treat them accurately and efficiently within the ML-MCTDH-SQR theory. It is also noted that the ML-MCTDH-SQR approach outlined above for fermions has also be formulated for bosons or combinations of fermions, bosons, and distinguishable particles.[65]

IV. RESULTS AND DISCUSSION

In this section, we present applications of the ML-MCTDH-SQR methodology to the study of correlated electron transport employing the model described in Sec. II. In particular, we discuss the influence of electron-electron and electronic-vibrational interaction on the transport characteristics for selected examples. Unlike the noninteracting transport model ($U_d = 0, c_j = 0$), these results represent nontrivial solutions to a many-body quantum problem and are often beyond the perturbation treatment. All calculations presented in this paper are for zero temperature, which corresponds to the deep quantum regime, and is often the most challenging physical regime of the problem. Meanwhile, this regime is relatively easy for our approach since only one initial wave function is required. An investigation of systems at finite temperature as well as an analysis of the physical mechanisms in a broader parameter range will be the topic of future work.

For all the calculations the variational parameters are systematically increased to achieve convergence according to the criterion that the stationary current should be converged with 10% relative error. In this paper a four-layer ML-MCTDH-SQR scheme has been employed. For the tight-binding parameters $\alpha_e = 0.2$ eV and $\beta_e = 1$ eV, a typical simulation requires, within the time scale of simulation, 128 discrete states per lead to represent the electronic continuum. With a smaller $\alpha_e = 0.1$ eV, 216 states per lead were used in most cases. The number of states used in the convergence tests ranges over 80-500. The numbers of the single particle functions for treating the electronic degrees of freedom are kept the same for all the layers in the ML-MCTDH-SQR simulation. This number ranges between 48 and 64, which is quite large comparing with ML-MCTDH simulations of other models. When the electron-vibration coupling is included, the phonon bath is discretized to 100-400 modes according the description in Sec. II. Here using 10 single particle functions for the phonon part (for all layers) is sufficient to achieve convergence.

A. Effect of electron-electron interaction on transport characteristics for fixed nuclei

We first focus on the influence of electron-electron interaction and consider models without electronic-vibrational

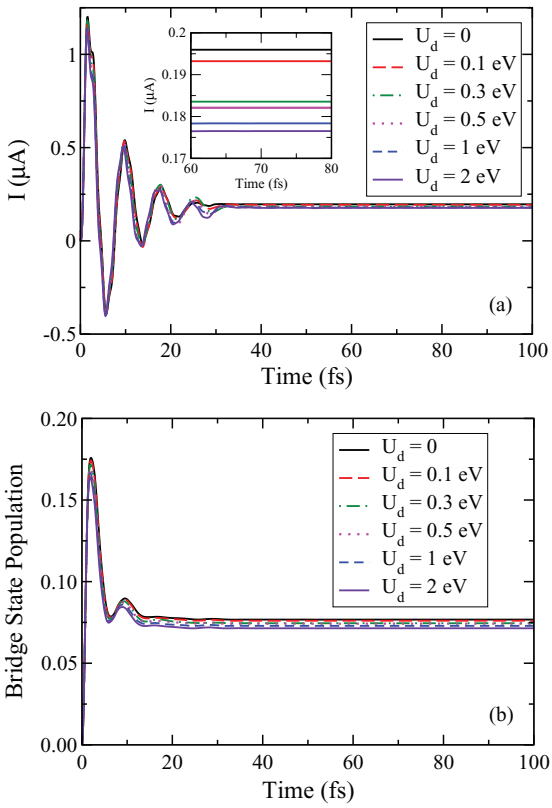

FIG. 1. (a) Time-dependent current $I(t)$ for different electron-electron coupling strength U_d and (b) the corresponding electronic population at the bridge state. Other parameters are: $\alpha_e = 0.2$ eV, $\beta_e = 1$ eV, $E_d - E_f = 0.5$ eV, and the source-drain voltage $V = 0.1$V. The inset in panel (a) depicts the stationary current in an enlarged view.

coupling ($c_j = 0$), i.e., for fixed nuclei. Figure 1 shows the time-dependent current and the corresponding bridge state population for a model with the following set of electronic parameters: The tight-binding parameters for the function $\Gamma(E)$ are $\alpha_e = 0.2$ eV, $\beta_e = 1$ eV, corresponding to a moderate molecule-lead coupling and a bandwidth of 4 eV. The energy of the bridge states E_d is located 0.5 eV above Fermi energy and the source-drain voltage is $V = 0.1$ V, i.e., the model is in the off-resonant transport regime. The results for both the current and the population show pronounced transient oscillations that decay on a time scale of $\approx\Gamma^{-1}$ ($\sim$4 fs) and approach a stationary plateau at longer times, which represents the steady state. The overall values of the current and population are rather small because the transport takes place in the off-resonant regime. The comparison of the results obtained for different parameters U_d shows that for this model electron-electron interaction has no significant influence on the population and the current, and this includes both the transient behavior and the long-time stationary value. Qualitatively this can be understood from the fact that the model is in the off-resonant transport regime. At zero coupling strength U_d, the bare energies of the electronic bridge states are the same and are outside the conductance window defined by the chemical potentials of the two electrodes. Including the on-site repulsion term removes the degeneracy of these two bridge states if one state is occupied. That is, when one of the bridge states is populated, the electronic energy of the other state is increased by the value of U_d. However, due to the fact that the initial bridge states are relatively far away from the conductance window, their populations are small. As a result, the overall electronic correlation effect is small for this set of model parameters. At a finer scale it can be seen that with the increase in U_d both the stationary current and bridge state population decreases. This is consistent with the fact that upon increasing U_d the energy of the doubly occupied state ($E_d + U_d$) is moved to higher energies and thus even further away from the conduction window.

Figure 2 shows the time-dependent current and the corresponding bridge state population for another model, where the parameters are the same as in Fig. 1 except for $E_d - E_f = 0$, i.e., the energy of the bridge states is located at the Fermi energy of the leads. For zero on-site coupling strength ($U_d = 0$), this set of parameters corresponds to the resonant tunneling regime and involves mixed electron/hole transport. This results in a significantly larger stationary current and a population of approximately one, because each bridge state has 50% probability to be occupied. In this parameter regime, electron-electron interaction has a pronounced influence on the transport characteristics. Upon increase of U_d the steady state value of both the current and the population decreases significantly. This is due to the fact that for increasing U_d the energy of the doubly occupied state moves out of the conductance window. For interaction strengths $U_d \gg 0.1$ eV, the bridge state can only be singly occupied, resulting in an overall population of $n_d = 1/2$, and the doubly occupied state does not contribute to the current.

We next consider in Figs. 3 and 4 a model with the same parameters as in the previous two cases except that the energy of the bridge state is below the Fermi energy, $E_d - E_f$

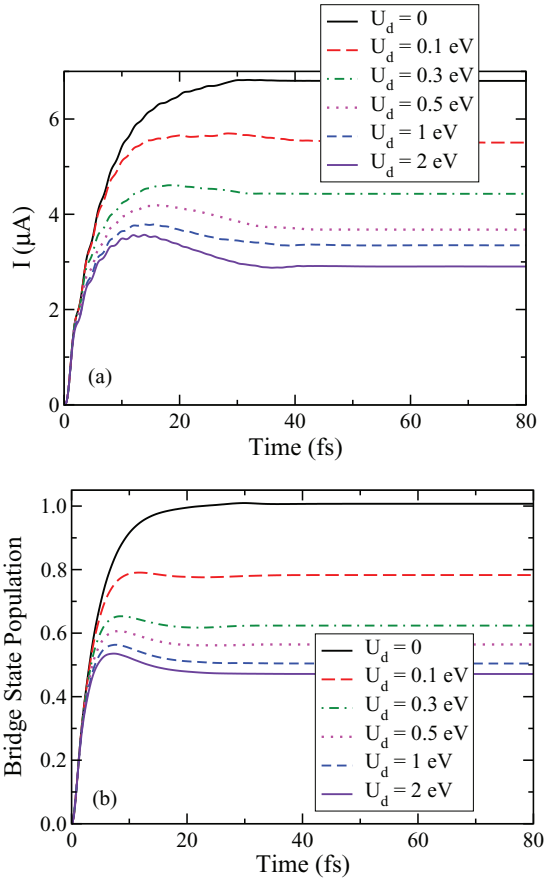

FIG. 2. Same as Fig. 1 except for $E_d - E_f = 0$.

$= -0.5$ eV. For vanishing electron-electron interaction, $U_d = 0$, this is again a non-resonant case. However, because the bridge state is, in contrast to Fig. 1, located below the Fermi energy it is almost doubly occupied when $U_d = 0$. While the stationary current for $U_d = 0$ (full black line in Fig. 3(a)) is, due to particle-hole symmetry, in fact identical to that in Fig. 1(a), the dependence of the transport characteristics on the electron-electron interaction is more complex than in the above two cases. Upon moderate increase of U_d, the energy of the doubly occupied state, $E_d + U_d$, moves closer to the Fermi energy and enters the conductance window. As a result, the population of this state decreases as shown in Fig. 3(b). The current (Fig. 3(a)), on the other hand, increases because the doubly occupied state provides a channel for resonant transport. It is also observed that upon moderate increase of U_d the transient dynamics undergoes a coherent to incoherent transition. When U_d is further increased ($U_d > 0.6$ eV), the energy of the doubly occupied state becomes higher than the chemical potentials of both electrodes. As shown in Fig. 4, this causes a decrease of the current and the population. For large values of U_d, the population in the steady state approaches a value of unity, because the bridge state can only be singly occupied. It is interesting to note that for large Coulomb repulsion, e.g., $U_d = 2$ eV, the initial transient current is negative. This is because in the simulation the bridge state is initially fully occupied. During the early transient time, electrons flow from the bridge states to both the left and the right electrodes, resulting in a negative transient current. As the bridge

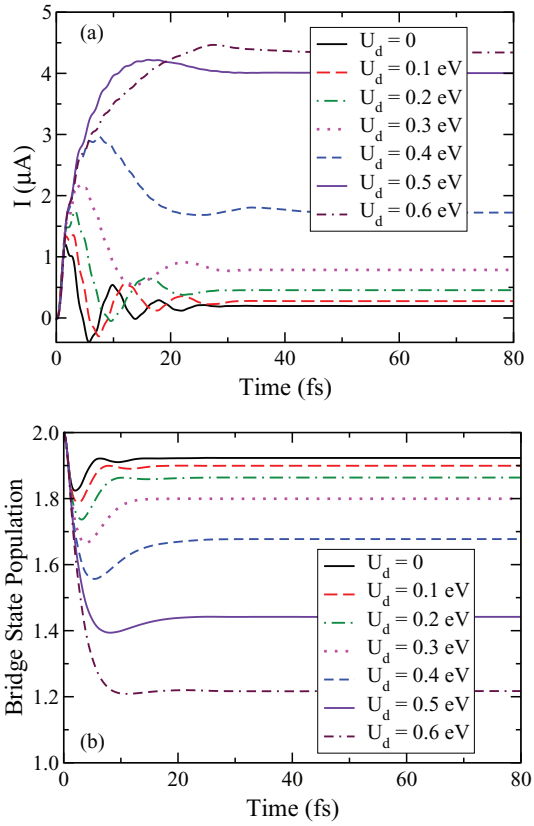

FIG. 3. Same as Fig. 1 except for $E_d - E_f = -0.5$ eV.

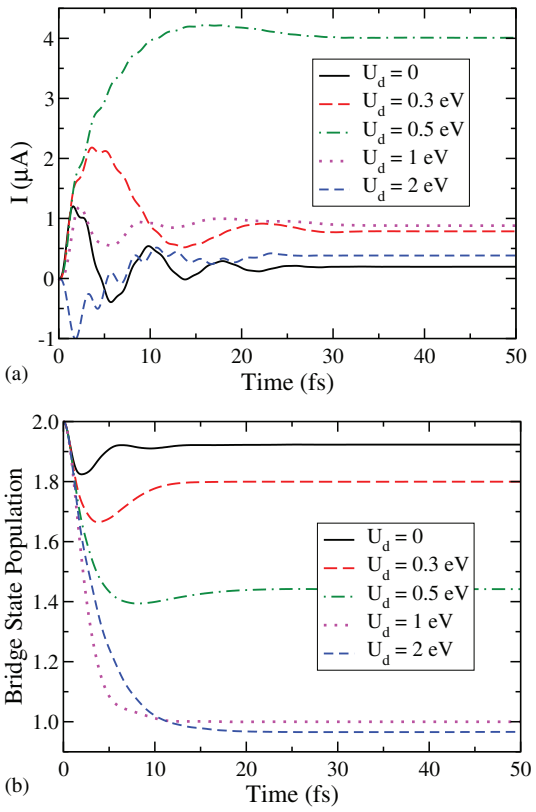

FIG. 4. Same as Fig. 3 except for a larger range of U_d.

states approach their steady state population, electrons move continuously from the left electrode to the right electrode, establishing a steady-state current.

B. Aspects of Coulomb blockade

An interesting many-body nonequilibrium effect in charge transport in mesoscopic and nanosystems is Coulomb blockade.[118–120] This phenomenon involves the suppression of the electrical current due to electron-electron interaction. Within the single-site Anderson impurity model, the underlying mechanism is that the Coulomb repulsion with an electron that already occupies the bridge state prevents a second electron to transfer onto the bridge and thus reduces the current compared to a noninteracting model.

This basic aspect of Coulomb blockade is demonstrated in Fig. 5, which shows simulated current-voltage characteristics for a resonant transport model, where the energy of the bridge states E_d is at the Fermi energy of the leads, $E_d - E_f = 0$. The tight-binding parameters for the function $\Gamma(E)$ are $\alpha_e = 0.1$ eV, $\beta_e = 1$ eV, corresponding to a smaller molecule-lead coupling and a bandwidth of 4 eV. Besides the noninteracting model ($U_d = 0$), three values of the electron-electron coupling strengths are considered: $U_d = 0.5$, 1, and 4 eV. To obtain the current-voltage characteristics, the stationary plateau value from the time-dependent simulation of the current was taken for each given voltage. The results show that upon inclusion of electron-electron interaction, the currents are suppressed at all voltages. The ratio between the blocked and unblocked currents attain a stationary value of approximately 2/3 in the plateau region (within the convergence range of less than 10% relative error), and is nearly independent of the electronic coupling strength U_d. Within a zeroth order picture, this result can be rationalized as follows.

For the model without electron-electron interaction ($U_d = 0$), there are three channels for electron transport through the two bridge states: (i) Electron transport through an initially unoccupied state. There are two such channels corresponding to the two spin polarizations of the bridge state. (ii) Electron transport through an initially singly occupied bridge resulting in the third channel which involves double occupation of the bridge state. When the source-drain voltage V is small, roughly $|eV| < 2U_d$ in the zeroth-order picture, the

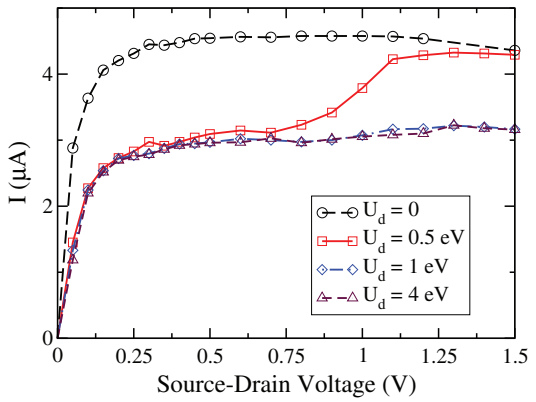

FIG. 5. Current-voltage characteristics for different electron-electron coupling strength U_d. Other parameters are: $\alpha_e = 0.1$ eV, $\beta_e = 1$ eV, $E_d - E_f = 0$. The lines are intended as a guide to the eye.

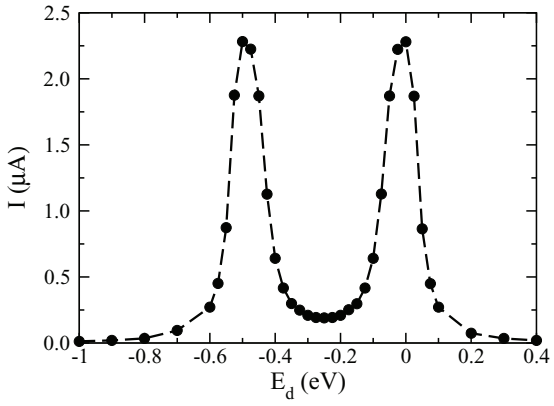

FIG. 6. Dependence of the current on the gate voltage. The electronic parameters are: $\alpha_e = 0.1$ eV, $\beta_e = 1$ eV, $U_d = 0.5$ eV, and $E_d - E_f = 0$ for zero gate voltage. The source-drain voltage is 0.1 V. The line is intended as a guide to the eye.

third two-electron transport channel is essentially closed, resulting in a current value 2/3 of that for the unblocked case. At approximately $|eV| = 2U_d$, e.g., $V = 1$ V for the case $U_d = 0.5$ eV in Fig. 5, the two-electron transport channel becomes available and the current begins to increase with the source-drain voltage. For finite molecule-lead coupling, the transition is broadened as shown in Fig. 5. For larger values of U_d, the energy of the doubly occupied state is outside the conductance window of the bias voltages considered and thus the current is suppressed.

While Fig. 5 demonstrates the phenomenon of Coulomb blockade for varying the source-drain voltage, it is also instructive to study the phenomenon for varying the gate voltage. Assuming that an additional gate voltage V_g predominantly shifts the energy of the bridge states E_d, we can investigate the influence of the gate voltage by varying E_d relative to the Fermi energy of the leads. The result depicted in Fig. 6 exhibits the well-known peak structures of Coulomb blockade, with maxima at energies $E_d = 0$ and $E_d = -U_d$, where the singly occupied levels and the doubly occupied level are in the conductance window, respectively. The parameters here are the same as in Fig. 5 except for a fixed $U_d = 0.5$ eV and a source-drain voltage $V = 0.1$V. It is noted that the value of the voltage considered is already beyond the linear response regime.

C. Effect of electron-electron interaction on transport characteristics in the presence of electron-vibrational coupling

We finally consider a model which includes both electron-electron and electron-vibrational interaction. The presence of both interactions increases the complexity significantly. To the best of our knowledge, the results presented here are the first numerical exact simulations for this type of models.

Figure 7 shows results for a model, where the electronic parameters are the same as in Fig. 2, i.e., $\alpha_e = 0.2$ eV, $\beta_e = 1$ eV, $E_d - E_f = 0$, and a source-drain voltage of $V = 0.1$ V. The electronic degrees of freedom are coupled to a vibrational

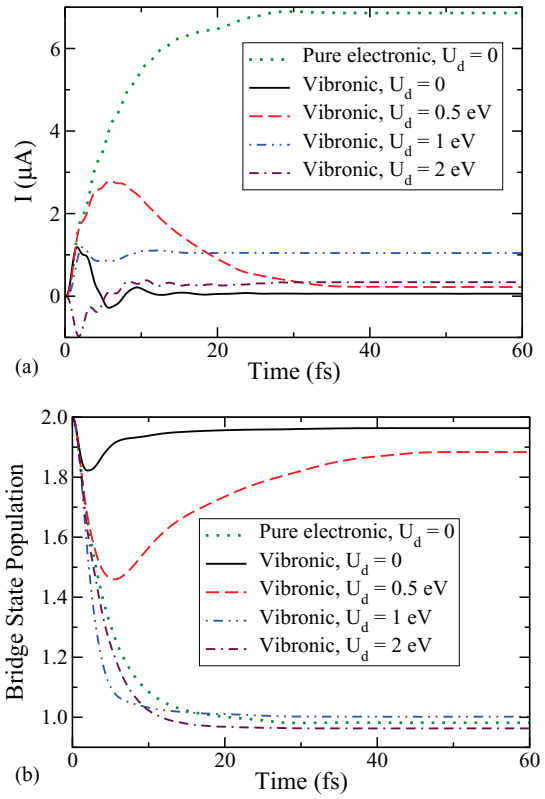

FIG. 7. (a) Time-dependent current $I(t)$ for different electron-electron coupling strength U_d and (b) the corresponding electronic population of the bridge state. The results are obtained for a model, which includes both electron-electron and electron-vibrational coupling. For comparison, result for a purely electronic model (i.e., $U_d = 0$, $\lambda = 0$) are shown as indicated in the legend. The source-drain voltage is $V = 0.1$ V. The electronic parameters are: $\alpha_e = 0.2$ eV, $\beta_e = 1$ eV, $E_d - E_f = 0$. The reorganization energy and characteristic frequency for the vibrational bath are $\lambda = 0.25$ eV and $\omega_c = 500\,\mathrm{cm}^{-1}$, respectively.

bath modeled by an Ohmic spectral density, as described in Sec. II. The characteristic frequency and the reorganization energy of the vibrational bath are $\omega_c = 500$ cm^{-1} and $\lambda = 2\alpha\omega_c = 0.25$ eV, respectively. These values are typical for larger molecular systems. Without Coulomb repulsion and coupling to the vibrational bath, this model corresponds to the resonant transport regime. Including the couplings to the vibrational modes has a significant impact on the electrical current. After a short transient time the coupling to the vibrations becomes effective and results in a suppression of the current. As illustrated by the solid black line in Fig. 7, the effect is very pronounced and the stationary current is essentially blocked. The underlying mechanism can be qualitatively rationalized by considering the energy level of the bridge states. For any finite bias voltage, the bare energy of the bridge states ($E_d - E_f = 0$) is located between the chemical potential of the leads and thus, within a purely electronic model, current can flow. The coupling to the vibrations results in a polaron shift of the energy of the bridge state given by the reorganization energy λ. For electronic-vibrational coupling strengths with $\lambda > |V|/2$ the polaron-shifted energy of the bridge state is below the chemical potentials of both leads and thus current is blocked. This effect, referred to as phonon blockade of the current, has been observed, e.g., in quantum dots[121] and has

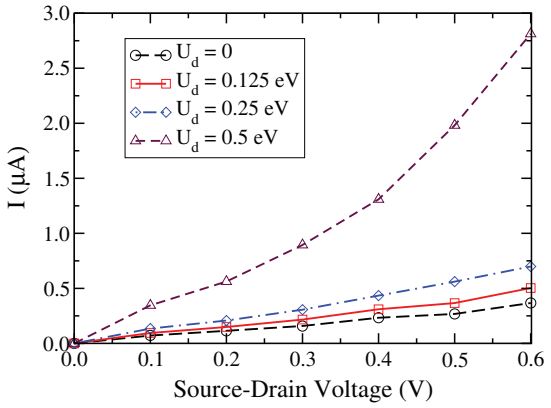

FIG. 8. Current-voltage characteristics for different electron-electron coupling strength U_d. The results are obtained for a model, which includes both electron-electron and electron-vibrational coupling. Other parameters are: $\alpha_e = 0.2$ eV, $\beta_e = 1$ eV, $E_d - E_f = 0$. The reorganization energy and characteristic frequency for the vibrational bath are $\lambda = 0.25$ eV and $\omega_c = 500\,\mathrm{cm}^{-1}$, respectively. The lines are intended as a guide to the eye.

been analyzed previously.[80] As shown in Fig. 7(b), the bridge states are almost fully occupied in this case.

When the Coulomb repulsion term is included in the simulation (in addition to the vibrational bath), the energy level of the doubly occupied bridge state is shifted to higher energies as discussed for the previous models. For smaller values of U_d, this brings the polaron-shifted bridge state back to the conduction window and thus increases the stationary current. This can be seen from the currents for $U_d = 0.5$ eV and $U_d = 1$ eV in Fig. 7(a) and in Fig. 8, which shows the current-voltage characteristics for a few selected values of U_d. It is evident that for small U_d the stationary current increases versus U_d.

However, if U_d becomes too large, e.g., $U_d = 2$ eV in Fig. 7(a), the doubly occupied bridge state has too high energy and is located above the conduction window, which again results in a suppression of the stationary current. On the other hand, the overall population of the bridge state decreases monotonically upon increase of U_d and reaches a value of unity for large U_d because then the bridge state can only be singly occupied. Due to the strongly correlated dynamics in this parameter regime, including both electron-electron and electronic-vibrational coupling, convergence for larger values of U_d and larger voltages than those depicted in Figs. 7 and 8 is difficult within our present implementation of the ML-MCTDH-SQR methodology. Experience shows that convergence in this regime can be facilitated by transforming the current Hamiltonian to another form in order to reduce correlation effects. This will be the subject of future work.

Although the interpretation of the above vibronic and electronic correlated transport properties is appealing in terms of the energetics of the bridge states, it should be emphasized that the mechanism involves the formation of correlated many-body states that are significantly more complex than this noninteracting electronic picture, and cannot be fully described by just considering the static shift of the energy of the bridge states. This is evident by examining the strength of the interaction parameters λ and U_d in Fig. 7. Thus, an accurate description of the vibrational and electronic dynamics as well as their couplings is essential to obtain a quantitative description of the many-body quantum dynamics and the transport characteristics.

V. CONCLUDING REMARKS

In this paper we have employed the ML-MCTDH-SQR method to study correlated electron transport through model single-molecule junctions. Extending our previous work,[65,80] we have considered models which include both electron-electron and electron-vibrational interaction. The ML-MCTDH-SQR method allows an accurate, in principle numerically exact treatment of this many-body quantum transport problem including both the transient dynamics and the steady state.

The results obtained for selected model systems demonstrate the complex interplay of electronic and vibrational dynamics. For example, strong electron-vibrational coupling may result in a pronounced suppression of the electrical current (phonon blockade), which is accompanied by the formation of a polaron-like state. Including electron-electron interaction, this suppression of the current can be partially lifted because the transport channel provided by the doubly occupied bridge state shifts into the conductance window.

In the present work we have considered a model with a single electronic state at the molecular bridge. It should be noted, however, that the ML-MCTDH-SQR method can also be applied to more complex models with various electronic states and interacting electrons in the leads. In addition to transport problems it may also be used to describe photoinduced dynamics in molecular adsorbates at metal or semiconductor surfaces including a proper description of correlation effects. Another important phenomenon in correlated electron transport is the Kondo effect.[29,78,122] The application of the methodology to simulate transport in the Kondo regime, in particular for very small voltage, requires special discretization techniques (e.g., the scheme pioneered by Wilson[123]) and can be facilitated by the use of correlated initial states. This will be considered in future work.

ACKNOWLEDGMENTS

This work has been supported by the National Science Foundation (NSF) through CHE-1012479 (H.W.), the German-Israeli Foundation for Scientific Development (GIF) (M.T.), and the Deutsche Forschungsgemeinschaft (DFG) through SFB 953 and the Cluster of Excellence "Engineering of Advanced Materials" (M.T.), and used resources of the National Energy Research Scientific Computing Center, which is supported by the Office of Science of the U.S. Department of Energy (DOE) under Contract No. DE-AC02-05CH11231. M.T. gratefully acknowledges the hospitality of the IAS at the Hebrew University Jerusalem within the workshop on molecular electronics.

[1] M. Reed, C. Zhou, C. Muller, T. Burgin, and J. Tour, Science **278**, 252 (1997).
[2] A. Nitzan and M. A. Ratner, Science **300**, 1384 (2003).
[3] C. Joachim, J. Gimzewski, and A. Aviram, Nature (London) **408**, 541 (2000).

[4] J. Cuevas and E. Scheer, *Molecular Electronics: An Introduction to Theory and Experiment* (World Scientific, Singapore, 2010).
[5] A. Nitzan, Annu. Rev. Phys. Chem. **52**, 681 (2001).
[6] G. Cuniberti, G. Fagas, and K. Richter, *Introducing Molecular Electronics* (Springer, Heidelberg, 2005).
[7] Y. Selzer and D. L. Allara, Annu. Rev. Phys. Chem. **57**, 593 (2006).
[8] F. Chen, J. Hihath, Z. Huang, X. Li, and N. Tao, Annu. Rev. Phys. Chem. **58**, 535 (2007).
[9] L. Venkataraman, J. E. Klare, C. Nuckolls, M. S. Hybertsen, and M. L. Steigerwald, Nature (London) **442**, 904 (2006).
[10] M. Galperin, M. A. Ratner, A. Nitzan, and A. Troisi, Science **319**, 1056 (2008).
[11] H. Park, J. Park, A. Lim, E. Anderson, A. Alivisatos, and P. McEuen, Nature (London) **407**, 57 (2000).
[12] X. Cui, A. Primak, X. Zarate, J. Tomfohr, O. Sankey, A. Moore, T. Moore, D. Gust, G. Harris, and S. Lindsay, Science **294**, 571 (2001).
[13] J. Park, A. Pasupathy, J. Goldsmith, C. Chang, Y. Yaish, J. Petta, M. Rinkoski, J. Sethna, H. Abruna, P. McEuen, and D. Ralph, Nature (London) **417**, 722 (2002).
[14] R. Smit, Y. Noat, C. Untiedt, N. Lang, M. van Hemert, and J. van Ruitenbeek, Nature (London) **419**, 906 (2002).
[15] J. Reichert, R. Ochs, D. Beckmann, H. Weber, M. Mayor, and H. von Lohneysen, Phys. Rev. Lett. **88**, 176804 (2002).
[16] N. Zhitenev, H. Meng, and Z. Bao, Phys. Rev. Lett. **88**, 226801 (2002).
[17] B. Xu and N. Tao, Science **301**, 1221 (2003).
[18] X. Qiu, G. Nazin, and W. Ho, Phys. Rev. Lett. **92**, 206102 (2004).
[19] N. Liu, N. Pradhan, and W. Ho, J. Chem. Phys. **120**, 11371 (2004).
[20] M. Elbing, R. Ochs, M. Koentopp, M. Fischer, C. von Hänisch, F. Weigend, F. Evers, H. Weber, and M. Mayor, Proc. Natl. Acad. Sci. U.S.A. **102**, 8815 (2005).
[21] S. Ballmann and H. B. Weber, New J. Phys. **14**, 123028 (2012).
[22] N. Ogawa, G. Mikaelian, and W. Ho, Phys. Rev. Lett. **98**, 166103 (2007).
[23] G. Schulze, K. J. Franke, A. Gagliardi, G. Romano, C. S. Lin, A. Da Rosa, T. A. Niehaus, T. Frauenheim, A. Di Carlo, A. Pecchia, and J. Pascual, Phys. Rev. Lett. **100**, 136801 (2008).
[24] F. Pump, R. Temirov, O. Neucheva, S. Soubatch, S. Tautz, M. Rohlfing, and G. Cuniberti, Appl. Phys. A **93**, 335 (2008).
[25] N. P. de Leon, W. Liang, Q. Gu, and H. Park, Nano Lett. **8**, 2963 (2008).
[26] E. A. Osorio, M. Ruben, J. S. Seldenthuis, J. M. Lehn, and H. S. J. van der Zant, Small **6**, 174 (2010).
[27] J. Hihath, C. Bruot, and N. Tao, ACS Nano **4**, 3823 (2010).
[28] C. A. Martin, J. M. van Ruitenbeek, and H. van de Zant, Nanotechnology **21**, 265201 (2010).
[29] W. Liang, M. Shores, M. Bockrath, J. Long, and H. Park, Nature (London) **417**, 725 (2002).
[30] J. Chen, M. Reed, A. Rawlett, and J. Tour, Science **286**, 1550 (1999).
[31] J. Gaudioso, L. J. Lauhon, and W. Ho, Phys. Rev. Lett. **85**, 1918 (2000).
[32] A. Blum, J. Kushmerick, D. Long, C. Patterson, J. Jang, J. Henderson, Y. Yao, J. Tour, R. Shashidhar, and B. Ratna, Nature Mater. **4**, 167 (2005).
[33] B.-Y. Choi, S.-J. Kahng, S. Kim, H. Kim, H. Kim, Y. Song, J. Ihm, and Y. Kuk, Phys. Rev. Lett. **96**, 156106 (2006).
[34] E. Lörtscher, J. W. Ciszek, J. Tour, and H. Riel, Small **2**, 973 (2006).
[35] C. Benesch, M. Cizek, J. Klimes, I. Kondov, M. Thoss, and W. Domcke, J. Phys. Chem. C **112**, 9880 (2008).
[36] H. Ness, S. Shevlin, and A. Fisher, Phys. Rev. B **63**, 125422 (2001).
[37] M. Cizek, M. Thoss, and W. Domcke, Phys. Rev. B **70**, 125406 (2004).
[38] M. Cizek, M. Thoss, and W. Domcke, Czech. J. Phys. **55**, 189 (2005).
[39] M. Caspary-Toroker and U. Peskin, J. Chem. Phys. **127**, 154706 (2007).
[40] J. Bonca and S. Trugmann, Phys. Rev. Lett. **75**, 2566 (1995).
[41] N. A. Zimbovskaya and M. M. Kuklja, J. Chem. Phys. **131**, 114703 (2009).
[42] R. Jorn and T. Seidemann, J. Chem. Phys. **131**, 244114 (2009).
[43] A. Mitra, I. Aleiner, and A. J. Millis, Phys. Rev. B **69**, 245302 (2004).
[44] M. Galperin, M. Ratner, and A. Nitzan, Phys. Rev. B **73**, 045314 (2006).
[45] D. A. Ryndyk, M. Hartung, and G. Cuniberti, Phys. Rev. B **73**, 045420 (2006).
[46] R. Härtle, C. Benesch, and M. Thoss, Phys. Rev. B **77**, 205314 (2008).
[47] R. Härtle, C. Benesch, and M. Thoss, Phys. Rev. Lett. **102**, 146801 (2009).
[48] K. Flensberg, Phys. Rev. B **68**, 205323 (2003).
[49] M. Tahir and A. MacKinnon, Phys. Rev. B **77**, 224305 (2008).
[50] J. P. Bergfield and C. A. Stafford, Phys. Rev. B **79**, 245125 (2009).
[51] T. Frederiksen, M. Paulsson, M. Brandbyge, and A. Jauho, Phys. Rev. B **75**, 205413 (2007).
[52] V. May, Phys. Rev. B **66**, 245411 (2002).
[53] J. Lehmann, S. Kohler, V. May, and P. Hänggi, J. Chem. Phys. **121**, 2278 (2004).
[54] J. N. Pedersen and A. Wacker, Phys. Rev. B **72**, 195330 (2005).
[55] U. Harbola, M. Esposito, and S. Mukamel, Phys. Rev. B **74**, 235309 (2006).
[56] A. Zazunov, D. Feinberg, and T. Martin, Phys. Rev. B **73**, 115405 (2006).
[57] L. Siddiqui, A. W. Ghosh, and S. Datta, Phys. Rev. B **76**, 085433 (2007).
[58] C. Timm, Phys. Rev. B **77**, 195416 (2008).
[59] V. May and O. Kühn, Phys. Rev. B **77**, 115439 (2008).
[60] V. May and O. Kühn, Phys. Rev. B **77**, 115440 (2008).
[61] M. Leijnse and M. R. Wegewijs, Phys. Rev. B **78**, 235424 (2008).
[62] M. Esposito and M. Galperin, Phys. Rev. B **79**, 205303 (2009).
[63] R. Härtle and M. Thoss, Phys. Rev. B **83**, 115414 (2011).
[64] R. Volkovich, R. Härtle, M. Thoss, and U. Peskin, Phys. Chem. Chem. Phys. **13**, 14333 (2011).
[65] H. Wang and M. Thoss, J. Chem. Phys. **131**, 024114 (2009).
[66] L. Mühlbacher and E. Rabani, Phys. Rev. Lett. **100**, 176403 (2008).
[67] S. Weiss, J. Eckel, M. Thorwart, and R. Egger, Phys. Rev. B **77**, 195316 (2008).
[68] D. Segal, A. J. Millis, and D. Reichman, Phys. Rev. B **82**, 205323 (2010).
[69] P. Werner, T. Oka, and A. J. Millis, Phys. Rev. B **79**, 035320 (2009).
[70] M. Schiro and M. Fabrizio, Phys. Rev. B **79**, 153302 (2009).
[71] F. B. Anders, Phys. Rev. Lett. **101**, 066804 (2008).
[72] F. Heidrich-Meisner, A. Feiguin, and E. Dagotto, Phys. Rev. B **79**, 235336 (2009).
[73] F. Jiang, J. Jin, S. Wang, and Y. Yan, Phys. Rev. B **85**, 245427 (2012).
[74] X. Zheng, J. Jin, S. Welack, M. Luo, and Y. Yan, J. Chem. Phys. **130**, 164708 (2009).
[75] G. Cohen and E. Rabani, Phys. Rev. B **84**, 075150 (2011).
[76] J. Eckel, F. Heidrich-Meisner, S. Jakobs, M. Thorwart, M. Pletyukhov, and R. Egger, New. J. Phys. **12**, 043042 (2010).
[77] P. Anderson, Phys. Rev. **124**, 41 (1961).
[78] A. Hewson, *The Kondo Problem to Heavy Fermions* (Cambridge University Press, Cambridge, UK, 1993).
[79] K. Albrecht, H. Wang, L. Mühlbacher, M. Thoss, and A. Komnik, Phys. Rev. B **86**, 081412(R) (2012).
[80] H. Wang, I. Pshenichnyuk, R. Härtle, and M. Thoss, J. Chem. Phys. **135**, 244506 (2011).
[81] C. Benesch, M. Rode, M. Cizek, R. Härtle, O. Rubio-Pons, M. Thoss, and A. Sobolewski, J. Phys. Chem. C **113**, 10315 (2009).
[82] A. J. Leggett, S. Chakravarty, A. T. Dorsey, M. P. A. Fisher, A. Garg, and W. Zwerger, Rev. Mod. Phys. **59**(1), 1 (1987).
[83] U. Weiss, *Quantum Dissipative Systems* (World Scientific, Singapore, 1993).
[84] H. Wang and M. Thoss, J. Chem. Phys. **119**(3), 1289 (2003).
[85] M. Thoss, H. Wang, and W. H. Miller, J. Chem. Phys. **115**(7), 2991 (2001).
[86] H. Wang, M. Thoss, and W. H. Miller, J. Chem. Phys. **115**(7), 2979 (2001).
[87] O. Gogolin and A. Komnik, e-print arXiv:condmat/0207513.
[88] M. Galperin, M. Ratner, and A. Nitzan, Nano Lett. **5**, 125 (2005).
[89] A. Alexandrov and A. Bratkovsky, J. Phys.: Condens. Matter **19**, 255203 (2007).
[90] E. Khosravi, A. Uimonen, A. Stan, G. Stefanucci, S. Kurth, R. van Leeuwen, and E. Gross, Phys. Rev. B **85**, 075103 (2012).
[91] A. Dzhioev and D. Kosov, J. Chem. Phys. **135**, 174111 (2011).
[92] A. Goldberg and B. W. Shore, J. Phys. B **11**, 3339 (1978).
[93] R. Kosloff and D. Kosloff, J. Comput. Phys. **63**, 363 (1986).
[94] D. Neuhauser and M. Baer, J. Chem. Phys. **90**, 4351 (1989).
[95] T. Seideman and W. H. Miller, J. Chem. Phys. **96**, 4412 (1992).
[96] J. Frenkel, *Wave Mechanics* (Clarendon Press, Oxford, 1934).
[97] H. Wang and M. Thoss, Chem. Phys. **370**, 78 (2010).
[98] M. Thoss and H. Wang, Chem. Phys. **322**(1–2), 210 (2006).
[99] H. Wang and M. Thoss, J. Chem. Phys. **124**(3), 034114 (2006).
[100] I. Kondov, H. Wang, and M. Thoss, J. Phys. Chem. A **110**(4), 1364 (2006).
[101] H. Wang and M. Thoss, J. Phys. Chem. A **111**, 10369 (2007).
[102] I. Kondov, M. Cizek, C. Benesch, H. Wang, and M. Thoss, J. Phys. Chem. C **111**(32), 11970 (2007).
[103] M. Thoss, I. Kondov, and H. Wang, Phys. Rev. B **76**, 153313 (2007).
[104] H. Wang and M. Thoss, Chem. Phys. **347**, 139 (2008).
[105] H. Wang and M. Thoss, New J. Phys. **10**, 115005 (2008).
[106] D. Egorova, M. F. Gelin, M. Thoss, H. Wang, and W. Domcke, J. Chem. Phys. **129**, 214303 (2008).
[107] K. A. Velizhanin and H. Wang, J. Chem. Phys. **131**, 094109 (2009).
[108] O. Vendrell and H.-D. Meyer, J. Chem. Phys. **134**, 044135 (2011).

[109]K. A. Velizhanin, H. Wang, and M. Thoss, Chem. Phys. Lett. **460**, 325 (2008).
[110]H. Wang, D. Skinner, and M. Thoss, J. Chem. Phys. **125**, 174502 (2006).
[111]I. R. Craig, M. Thoss, and H. Wang, J. Chem. Phys. **127**, 144503 (2007).
[112]U. Manthe, J. Chem. Phys. **128**, 164116 (2008).
[113]U. Manthe, J. Chem. Phys. **130**, 054109 (2009).
[114]T. Kato and H. Kono, Chem. Phys. Lett. **392**, 533 (2004).
[115]J. Caillat, J. Zanghellini, M. Kitzler, O. Koch, W. Kreuzer, and A. Scrinzi, Phys. Rev. A **71**, 012712 (2005).
[116]M. Nest, T. Klamroth, and P. Saalfrank, J. Chem. Phys. **122**, 124102 (2005).
[117]O. E. Alon, A. I. Streltsov, and L. S. Cederbaum, Phys. Rev. A **77**, 033613 (2008).
[118]L. Glazman and R. Shekhter, J. Phys. Condens. Matter **1**, 5811 (1989).
[119]C. Beenakker, Phys. Rev. B **44**, 1646 (1991).
[120]H. Grabert and M. H. Devoret, *Single Charge Tunneling: Coulomb Blockade Phenomena in Nanostructures* (Plenum, New York, 1992).
[121]E. Weig, R. Blick, T. Brandes, J. Kirschbaum, W. Wegscheider, M. Bichler, and J. P. Kotthaus, Phys. Rev. Lett. **92**, 046804 (2004).
[122]W. van der Wiel, S. Franceschi, T. Fujisawa, J. Elzerman, S. Tarucha, and L. Kouwenhoven, Science **289**, 2105 (2000).
[123]K. Wilson, Rev. Mod. Phys. **47**, 773 (1975).